Hindawi
Shock and Vibration
Volume 2023, Article ID 7400955, 10 pages
https://doi.org/10.1155/2023/7400955

*Research Article*

# Effect of Track Support Structures on Friction-Induced Vibrations of Wheelset-Track Systems

**Hua Fu**,[1] **Fei Kang**,[1,2] **Shanglin Liu**,[1] **and Xi Kang**[3]

[1]*Faculty of Electrical and Control Engineering, Liaoning Technical University, Huludao 125100, China*
[2]*Human Resources Office, Liaoning Guidao Jiaotong Polytechnic Institute, Shenyang 110000, China*
[3]*School of Advanced Manufacturing Engineering, Chongqing University of Posts and Telecommunications, Chongqing, China*

Correspondence should be addressed to Hua Fu; fxfuhua@163.com and Shanglin Liu; authorchnlsl@163.com

Received 17 February 2023; Revised 6 July 2023; Accepted 25 July 2023; Published 14 August 2023

Academic Editor: Lutz Auersch



The aim of the present investigation is to study the effect of track support structures on the metro 5th to 8th-order out-of-round (OOR) wheel caused by friction-induced vibrations. Three finite element models of metro-leading wheelset-track systems with three types of track support structures were established. The motion stabilities of these systems were studied using the complex feature value method. Three unstable vibrations that may cause the formation of the 5th to 8th order wheel OOR profiles were predicted. The simulation results show that the saturated creep forces can lead to unstable vibrations of wheelset-track systems, which are capable of inducing the 5th to 8th-order OOR wheel shapes. Choosing the appropriate value of the fastener damping and using the rail dampers are helpful to reduce or even eliminate wheel polygonal wear caused by these vibrations.

## 1. Introduction

In recent years, many cities in China have built new subway lines. However, due to the complexity of some subway lines and the diversity of train operating environments, the wheel-rail interaction in some sections is extremely intense, resulting in the formation of out-of-round (OOR) wheels. Wheel polygonization is a typical periodic wheel out-of-roundness, and the order of this OOR wheel refers to the number of peaks of the wheel polygonal profile. When a metro train with OOR wheels runs, there are severe vibrations and noises making passengers uncomfortable. These vibrations also can cause fatigue fractures of some vehicle and track components [1, 2]. So far, there is no agreement on the generation mechanism of OOR wheels [3–7]. Meinke et al. [8] established a 40-DOF dynamical model with a high-speed wheelset. In this model, the wheelset was regarded as a spring-supported rotor, and the wheel-rail system was regarded as a roller bearing. The effect of imbalances on wheelset vibrations and wheel tread wear was studied. The results showed that the wheel tread suffered from polygonal wear when the unbalanced wheelset operated at a high speed. Morys [9] studied the development of an initial wheel corrugation using an ICE-1 vehicle-track dynamical model. A wear model was established to simulate the evolution of radius deviations between the two wheels of the same wheelset over a long-term operation. The results showed that when a wheelset with an initial wheel corrugation ran on a track supported by a high stiffness fastener, wheel-rail normal contact forces varied acutely, thus inspiring the bending resonance of the wheelset. This resonance can cause lateral slip and material wear of the wheels, leading to the generation of OOR wheel profiles. Based on the high-frequency vibrations of the wheel-rail system and track irregularity, Nielsen et al. [10] studied the short-pitch rail corrugation occurring on smooth curved tracks or on straight tracks, wheel uneven wear caused by pad-wheel braking, and polygonalization of wheel treads. Some inhibition measures were proposed. Johansson and Andersson [11] used a multibody system model to simulate the wheel-rail interaction, using an iterative approach to input the feedback from these simulation results into a long-term wear model and proposed a method for predicting the wheel polygonal wear. Simulation results showed that the

frequency-fixing mechanisms causing the development of OOR wheels were the wheel-rail vertical resonance of around 40 Hz, the P2 resonance, and the vertical track antiresonance of frequency of about 165 Hz. Dekker [12] studied the phenomenon of wheel polygonal wear by building a nonrigid vehicle-track vibrational model, and he found that the enhancement of a vibrational wheel instability led to the increase of the polygonization of wheels. Increasing the train mass can reduce this nuisance. Wei et al. [13] established a railway vehicle dynamics model with flexible wheelsets to study the generation mechanism of metro OOR wheels. The bending mode of the wheelset coupling with the bounce motion of the liner motor can lead to wheel polygonal wear. Many vibration tests of vehicles and tracks have been performed by Tao et al. [14] in Chinese subway lines. The results showed that the direction of the curved track as well as track support structures had important effects on the formation of the 5th to 8th-order OOR wheels. Wu et al. [15] analyzed the stability of a wheelset-track system with axle-mounted disc brake units by using the complex eigenvalue method. Simulation results showed that the unstable vibrations of frequencies from 580 Hz to 650 Hz caused by axle-mounted disc braking may be transmitted to wheel-rail systems, thus inducing the 20th to 23rd-order polygonal wear on high-speed train trailer wheels. Zhao et al. [16] established a finite element model of a subway wheelset-rail system. When the wheelset is operated on a tightly curved track, frictional self-excited vibrations that may occur on this system were predicted, causing the formation of OOR wheels. The relative error of this prediction method was analyzed by comparing the results of field measurement and model simulation [17].

Some subway lines in China use different track support structures [18] due to different operating environments, including different fasteners and sleepers. Previous field measurements [17] have shown that in Beijing Metro Line 4, the main vibrational frequencies of the three track test sites supported by different track support structures are different when a metro train is passing. In addition, changing the track support structure, such as reducing the fastener stiffness [14], may be effective in suppressing the 5th to 8th-order OOR wheel. Therefore, it is helpful for understanding the formation mechanism of metro OOR wheels to study the effect of track support structures on the wheel-rail interaction.

When a metro train runs on a tightly curved track, wheel-rail creep forces of the leading wheelset easily reach saturation [19]. The authors believe that these forces may lead to unstable self-excited vibrations in wheel-rail systems, causing the periodical lateral slip between the rail head and the wheel tread, thus inducing the wheel polygonal wear.

The finite element model is usually used to study the system stability [20], wheel-rail contact [21], and railway noise and vibrations [22]. The differences in the research objects lead to differences in modelling and analysis methods. In this paper, the fasteners were simulated by a new method in finite element models. According to the frequency-fixing mechanism and the mode analysis, it can be found that frictional self-excited vibrations may be a cause of metro wheel polygon wear.

## 2. Numerical Modelling of Leading Wheelset-Track Systems

*2.1. Finite Element Modelling.* Figure 1 shows the three types of sharp curved ballastless tracks supported by different track support structures in a metro line (line A) [18], including a track with DTVI fasteners and short sleepers (type 1), a track with cologne-egg fasteners (type 2), a track with type-II fasteners, and rubber-booted short sleepers (type 3). The rail profile is the CN60, and the wheel profile is the LM worn-type. The values of the stiffness and damping of these fasteners [18] are shown in Table 1.

Figure 2 shows the finite element models of the leading wheelset-track systems with different types of tracks [23]. In these models, a series of equivalent spring and viscous damping elements are, respectively, established to simulate the support stiffness and damping of fasteners, slabs, and the subgrade. In the model with the track type 1, as shown in Figure 2(a), the short sleepers are fixed on slabs by using the tie constraint. This constraint is also used to simulate bolts connecting iron pads of fasteners with sleepers. There is no sleeper in the model with track type 2 [24], as shown in Figure 2(b), so the bolts connect iron pads to slabs. The model with track type 3 is shown in Figure 2(c), and in this model, rubber boots connecting the short sleepers to the slabs are modelled as the spring and damping elements [25]. Values of the main parameters of these finite element models are shown in Table 2 [19].

## 3. Numerical Method for Friction-Induced Vibration

The motion equation of a wheel-rail system without friction is expressed by the following formula [26]:

$$M\ddot{x} + C\dot{x} + Kx = 0, \tag{1}$$

where $M$, $C$, and $K$ are, respectively, the mass, damping, and stiffness symmetric matrixes, and $x$ is the nodal displacement vector. There is no positive real part eigenvalue in the solution of the corresponding eigenvalue equation, so this system is stable. The friction equation is as follows:

$$F = \mu N, \tag{2}$$

where $F$ is the friction, $\mu$ is the friction coefficient, and $N$ is the normal contact force. The value of $\mu$ can be obtained by using the following formula:

$$\mu = \mu_s + u v_1, \tag{3}$$

where $\mu_s$ is the static friction coefficient, $u$ is the friction-velocity slope, and $v_1$ is the wheel-rail relative sliding speed. Then, the motion equation of the system with friction becomes

$$\left(M - M_f\right)\ddot{x} + \left(C + C_f + C_u\right)\dot{x} + \left(K + K_f\right)x = \Delta N, \tag{4}$$

where $M_f$ is the friction influence matrix of mass, $C_f$ is the friction influence matrix of damping, $C_u$ is the friction-velocity slope influence matrix of damping, and $K_f$ is the friction

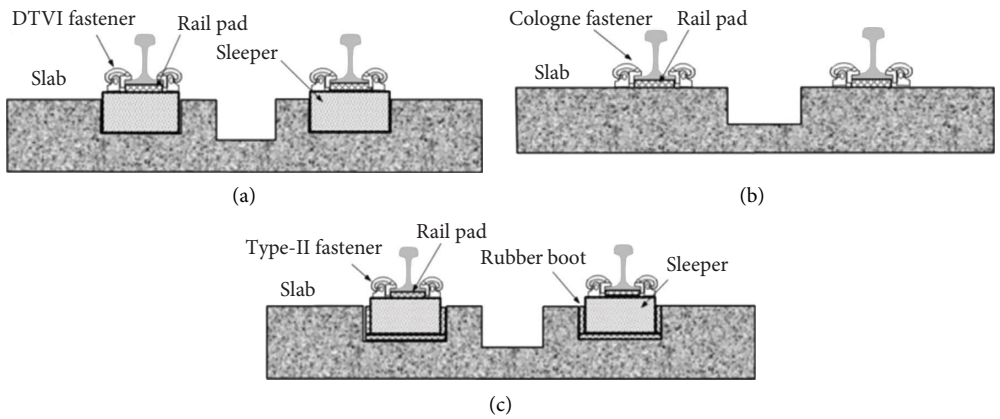


Figure 1: Three types of tightly curved tracks supported by different track support structures in line A [18]: (a) track type 1, (b) track type 2, and (c) track type 3.

Table 1: Parameters of fasteners used in the three types of tracks [18].

| Track type | Fastener type | Lateral | | Vertical | |
|---|---|---|---|---|---|
| | | Stiffness (MN/m) | Damping (kNs/m) | Stiffness (MN/m) | Damping (kNs/m) |
| 1 | DTVI | 8.79 | 1.93 | 40.73 | 9.90 |
| 2 | Cologne-egg | 7.58 | 0.97 | 12.07 | 1.36 |
| 3 | Type-II | 9.00 | 1.83 | 18.28 | 6.36 |

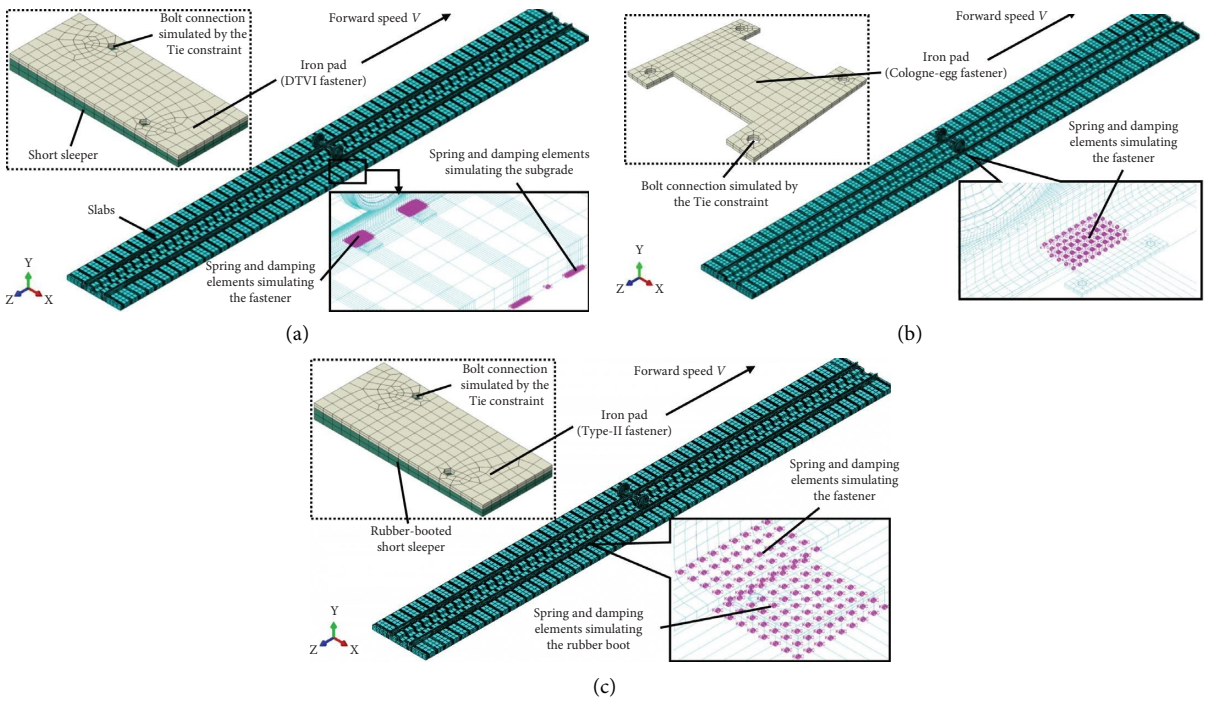


Figure 2: Finite element models of a leading wheelset-track system with (a) track type 1, (b) track type 2, and (c) track type 3.

influence matrix of stiffness. $\Delta N$ is the normal force disturbance vector. The simplified motion equation is as follows:

$$M_r\ddot{x} + C_r\dot{x} + K_r x = 0, \tag{5}$$

where $M_r$, $C_r$, and $K_r$ are the mass, damping, and stiffness asymmetric matrixes, respectively. The eigenvalue equation of equation (5) can be solved according to the QZ method, and the general solution is

Table 2: Values of the main parameters of finite element models [19].

| Parameter | Value |
|---|---|
| *Leading wheelset* | |
| Outer vertical suspension force (N) | 53,681 |
| Inner vertical suspension force (N) | 49,164 |
| Outer lateral suspension force (N) | 233 |
| Inner lateral suspension force (N) | 204 |
| Density of wheelset (kg/m$^3$) | 7790 |
| Young's modulus of wheelset (N/m$^2$) | $2.059 \times 10^{11}$ |
| Poisson's ratio of wheelset | 0.3 |
| *Rail* | |
| Length of rail (m) | 36 |
| Sleeper spacing (m) | 0.625 |
| Radius (m) | 350 |
| Density of rail (kg/m$^3$) | 7790 |
| Young's modulus of rail (N/m$^2$) | $2.06 \times 10^{11}$ |
| Poisson's ratio of rail | 0.3 |
| Wheel-rail friction coefficient $\mu_1$ | 0.4 |
| *Track support structures* | |
| Density of iron pads (kg/m$^3$) | 7790 |
| Young's modulus of iron pads (N/m$^2$) | $2.06 \times 10^{11}$ |
| Poisson's ratio of iron pads | 0.3 |
| Density of sleepers and slabs (kg/m$^3$) | 2400 |
| Young's modulus of sleepers and slabs (N/m$^2$) | $3.25 \times 10^{10}$ |
| Poisson's ratio of sleepers and slabs | 0.24 |
| Iron pad-sleeper friction coefficient | 0.75 |
| Support stiffness from subgrade (MN/m) | 491 |
| Support damping from subgrade (kNs/m) | 90 |

$$x(t) = \sum_{i=1}^{n} f_l \exp(\alpha_i + j\omega_i)t, \tag{6}$$

where $\alpha_i + j\omega_i$ is the eigenvalue and $t$ is the time. As can be seen from the general solution, the nodal displacement will increase over time if $\alpha_i$ is greater than 0, and an unstable vibration may occur in the system. The effective damping ratio $\xi$ for quantifying the tendency of the unstable vibration is defined as

$$\xi = -\frac{2\alpha_i}{(|\omega_i|)}, \tag{7}$$

when $\xi$ is less than −0.001, the unstable vibration can overcome the damping of the system. The smaller the effective damping ratio, the stronger the trend of the unstable vibration occurring in the system.

## 4. Results

*4.1. Unstable Vibration of Leading Wheelset-Track Systems.* When a metro train passes through a tightly curved track in China, the speed $V_c$ of this train changes from 45 to 55 km/h [19], the wheel diameter is about 0.84 m, and the dominating wavelengths $\lambda$ of the wheel of the 5th to 8th-order polygon are from 330 to 530 mm [14]. Therefore, the OOR wheel passing frequency range can be computed as follows:

$$f_c = \frac{V_c}{\lambda} = \frac{45 \sim 55\text{km/h}}{330 \sim 530\text{mm}} \approx 24 \sim 46\text{Hz}. \tag{8}$$

Distributions of unstable vibrations of leading wheelset-track systems within the frequency domain were obtained by complex eigenvalue analysis, as shown in Figure 3. In the frequency range of 0~600 Hz, five unstable vibrations occur in the system with track type 1, as shown in Figure 3(a). The minimum frequency of these vibrations is about 51 Hz which is larger than 46 Hz, so it is clear that all vibrations are not within the frequency range of 24~46 Hz which may cause the 5th to 8th-order OOR wheel. However, the vibrations of frequencies of about 51 Hz, 60 Hz, and 69 Hz may be related to the 9th-order' OOR wheel [19, 27]. Figure 3(b) shows the distribution of unstable vibrations of the system with track type 2. There is a vibration of frequency of about 41 Hz within the 5th to 8th-order OOR wheel passing frequency range, and the effective damping ratio of this vibration is the smallest, with a value of −0.05243. It means that this unstable vibration of frequency of about 41 Hz is more likely to occur than other unstable vibrations in this system. Figure 3(c) shows the distribution of unstable vibrations of the system with track type 3. The unstable vibrations of frequencies of about 35 Hz and 42 Hz may cause the 5th to 8th-order wheel polygonal wear. The vibration of frequency of about 42 Hz has the smallest effective damping ratio with a value of −0.09092, which means that it is more likely to occur than other unstable vibrations in this system.

In summary, there are three unstable vibrations that may lead to the formation of the 5th to 8th-order wheel OOR shapes, which have the frequencies of about 35 Hz, 41 Hz, and 42 Hz, respectively. Modes of these unstable vibrations are, respectively, shown in Figures 4(a)–4(c), and these vibrations mainly occur in wheels and rails. As can be seen from the details (the direction of the red arrow is the direction of the nodal displacement in the finite element model, and the length of the arrow represents the size of the nodal displacement), each low rail is obviously deformed. The deformation of the low rail can be described by the low rail outlines indicated by the broken line in Figure 4(d). The inner wheel tread slips laterally on the low rail head due to this deformation, which causes wear at the contact position of the wheel treads away from the wheel back. It should be noted that the slip is periodical, and the period is the same as that of the unstable vibration. Moreover, from Figure 4, it can be seen that the rail rigidly rotates around the $z$-axis instead of any elastic deformation (like at curve squealing). As a result, the 5th to 8th-order polygonal wear is formed on the inner wheel tread. In addition, there is no obvious lateral slip between the high rail head and the outer wheel tread, and the contact point between them is near the wheel flange. Therefore, it is difficult for the unstable vibration to cause polygonal wear on the outer wheel tread.

The speed $V_t$ of the metro train operating on a tangential track often changes from 60 to 75 km/h in line A, and the range of the vibration frequency caused by the 5th to 8th-order OOR wheel shapes can be computed as follows:

$$f_t = \frac{V_t}{\lambda} = \frac{60 \sim 75\text{km/h}}{330 \sim 530\text{mm}} \approx 31 \sim 63\text{Hz}. \tag{9}$$

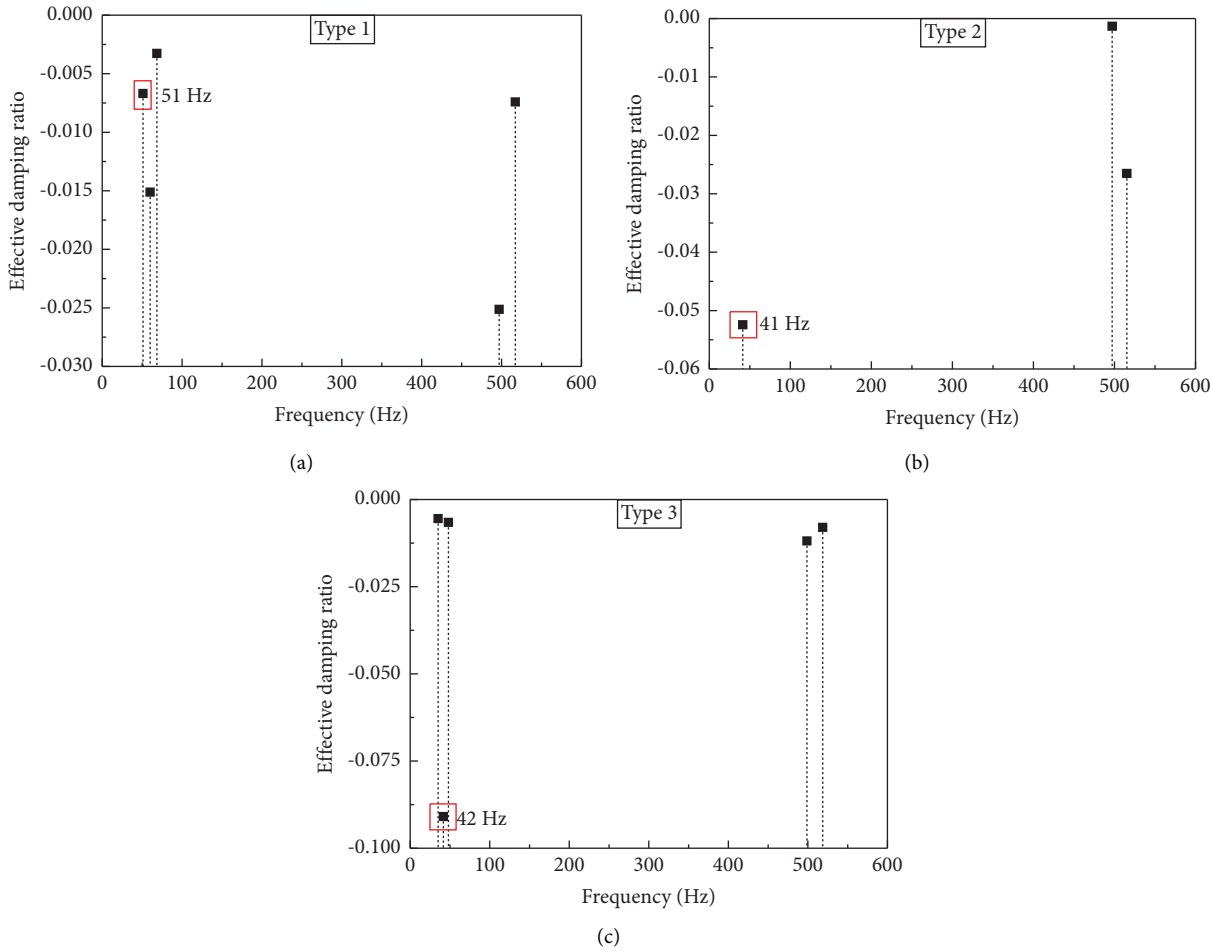


Figure 3: Distributions of unstable vibrations of the leading wheelset-track system with (a) track type 1, (b) track type 2, and (c) track type 3.

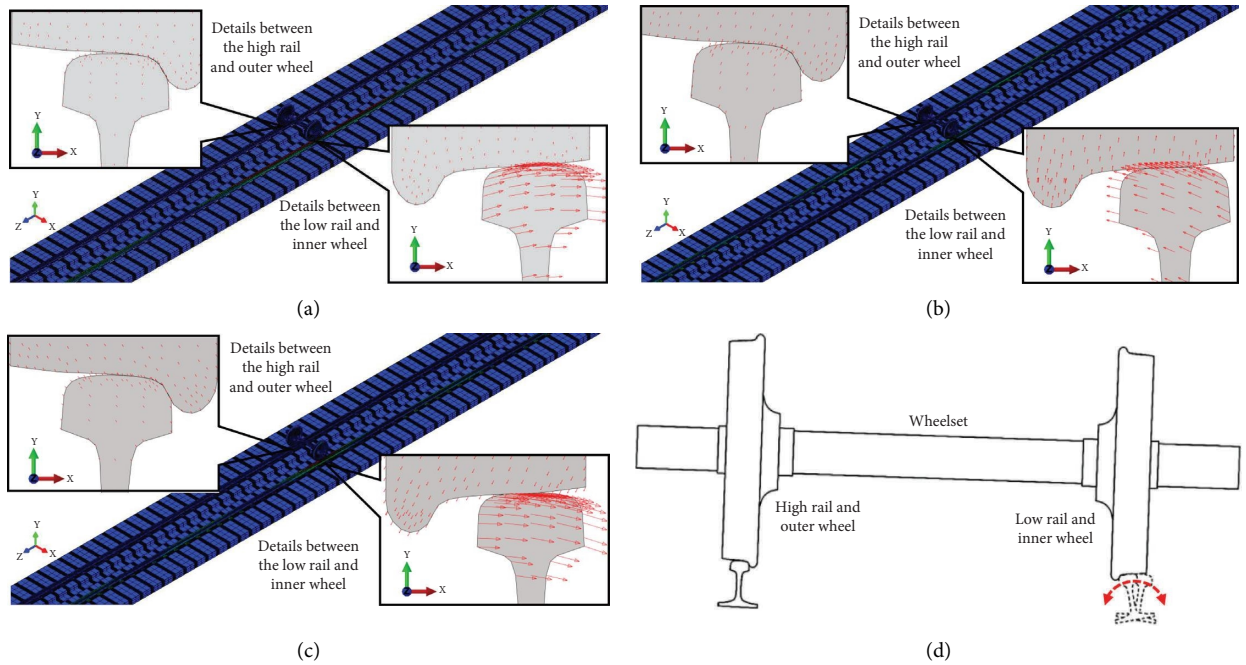


Figure 4: Modes of unstable vibrations of the leading wheelset-track system with (a) track type 2: frequency $f \approx 41$ Hz, (b) track type 3: frequency $f \approx 35$ Hz, (c) track type 3: frequency $f \approx 42$ Hz, and (d) lateral slip causing polygonal wear on the inner wheel treads.

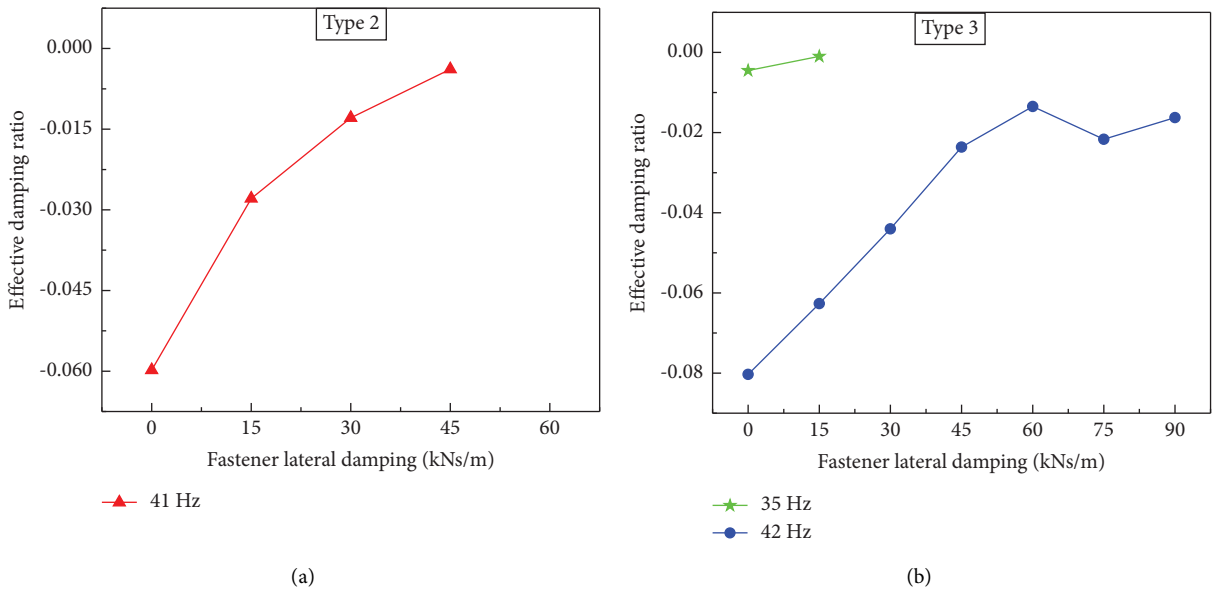


Figure 5: Effect of the fastener lateral damping on unstable vibrations of the leading wheelset-track system with (a) track type 2 and (b) track type 3.

The P2 resonance with a frequency of 50~80 Hz may be excited by this vibration, thus exacerbating the wheel's polygonal wear [14]. After a long-time service, the 5th to 8th-order OOR wheel is gradually formed.

## 5. Effect of Fastener Damping

The lateral damping and vertical damping of fasteners are mainly provided by rail rubber pads, and they vary over time due to rubber ageing. In order to study the effect of fastener damping on the unstable vibrations which may cause the formation of the 5th to 8th-order wheel OOR shapes, different values of fastener damping were, respectively, set in the wheelset-track systems with track type 2 and track type 3. When the value of one damping (lateral or vertical) changes within the range from 0 to 90 kNs/m, the value of another damping remains unchanged.

As shown in Figure 5(a), when the value of the lateral damping increases to 45 kNs/m from 0 kNs/m in the wheelset-track system with track type 2, the effective damping ratio of unstable vibration of frequency of about 41 Hz rises to −0.00386 from −0.05980. When the value of the lateral damping increases to 60 kNs/m or greater, this unstable vibration disappears. When the value of the lateral damping increases to 15 kNs/m from 0 kNs/m in the system with track type 3, as shown in Figure 5(b), the effective damping ratio of unstable vibration of frequency of about 35 Hz rises to −0.00098 from −0.00453, and this vibration disappears when the value of the lateral damping increases to 30 kNs/m or greater. In addition, the effective damping ratio of unstable vibration of frequency of about 42 Hz rises to −0.01348 from −0.08032 when the value of the lateral damping increases to 60 kNs/m from 0 kNs/m. However, when the value of the lateral damping increases continually to 75 kNs/m, the effective damping ratio decline slightly to −0.02165, and then it increases to −0.01626 when the value of the lateral damping increases to 90 kNs/m. This means that when the value of the lateral damping is 60 kNs/m, the occurrence likelihood of this unstable vibration is the lowest. Therefore, it can be concluded that increasing the value of the lateral damping to 60 kNs/m is helpful to reduce or even eliminate the 5th to 8th-order OOR wheel caused by the friction-induced vibrations.

When the value of the vertical damping increases to 7.5 kNs/m from 0 kNs/m in the system with track type 2, as shown in Figure 6(a), the effective damping ratio of unstable vibration of frequency of about 41 Hz rises to −0.00544 from −0.0685. This unstable vibration disappears when the value of the vertical damping increases to 10 kNs/m or greater. In Figure 6(b), when the value of the vertical damping increases to 7.5 kNs/m from 0 kNs/m in the system with track type 3, the effective damping ratio of unstable vibration of frequency of about 35 Hz increases to −0.00411 from −0.00955, and this vibration disappears when the value of the vertical damping increases to 15 kNs/m or greater. The effective damping ratio of another unstable vibration of frequency of about 42 Hz rises to −0.00825 from −0.11468 when the value of the vertical damping increases to 37.5 kNs/m from 0 kNs/m. When the value of the vertical damping increases to 45 kNs/m or greater, this unstable vibration disappears. Therefore, properly choosing the value of the vertical damping can suppress the formation of the 5th to 8th-order OOR wheel.

*5.1. Effect of Rail Dampers.* Field tests and simulations have proved that the installation of rail dampers can effectively inhibit the formation of noise and rail corrugation [28–30], such as the Beijing Metro Line 6 and Shenzhen Metro Line 1 [31] in China. In order to study the effect of rail dampers on unstable vibrations, the finite element model of rail dampers was built. The rail damper consists of a mass bar and the

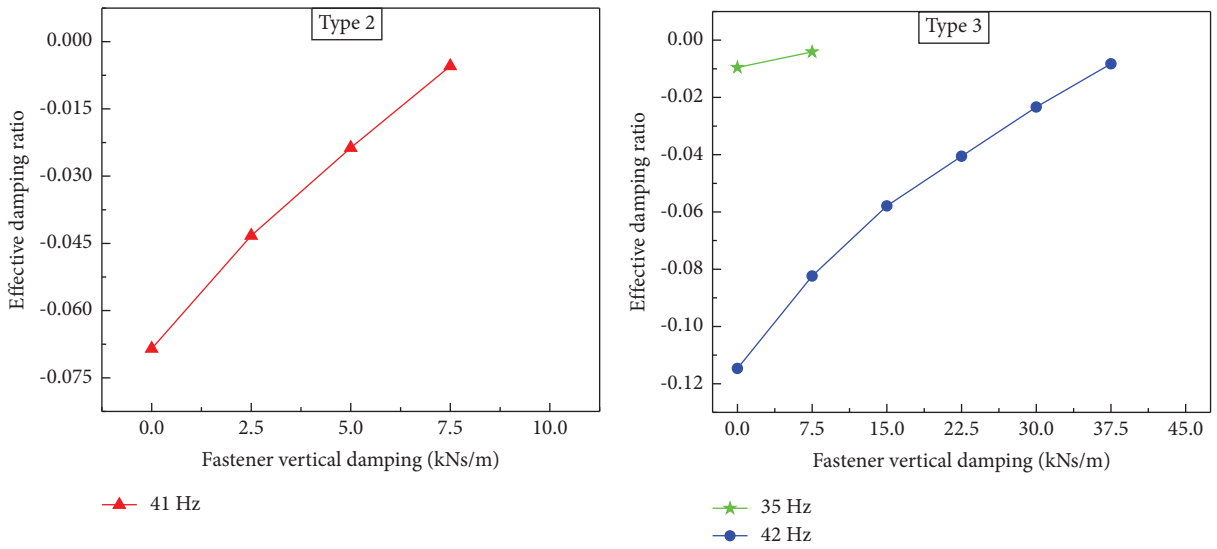


FIGURE 6: Effect of the fastener vertical damping on unstable vibrations of the leading wheelset-track system with (a) track type 2 and (b) track type 3.

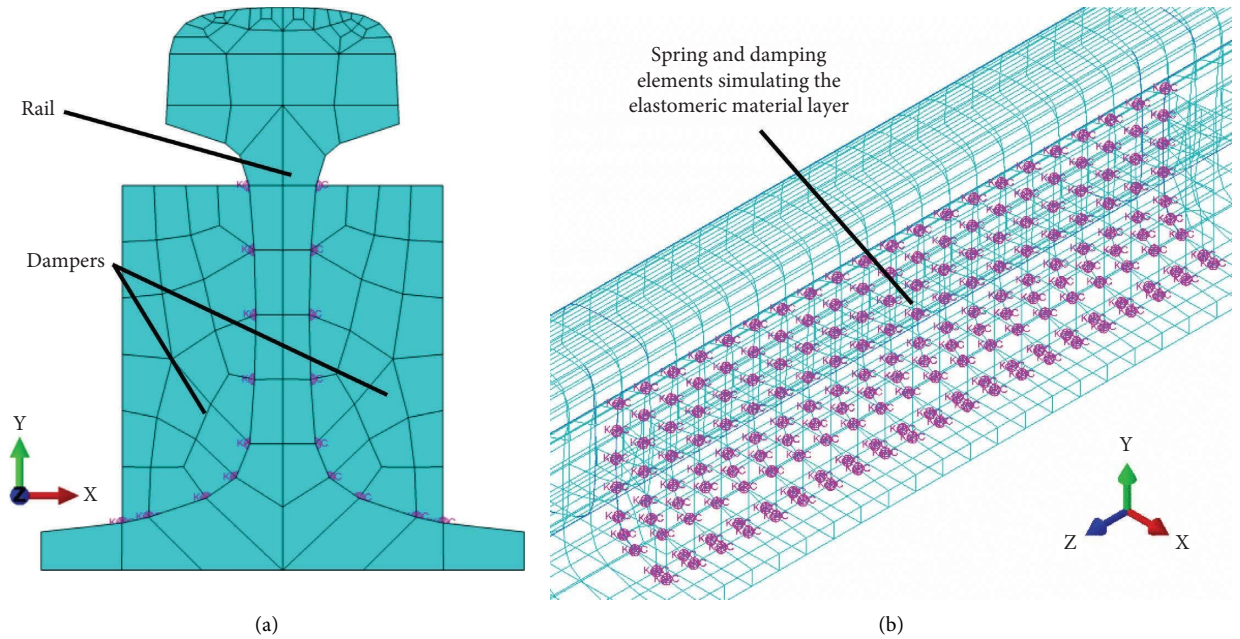


FIGURE 7: Finite element model of a rail with rail dampers: (a) front view and (b) connection details.

elastomeric material layer. The mass bar was established as an elastomer, and its density, Young's modulus, and Poisson's ratio are 7850 kg/m$^3$, $1.9 \times 10^{11}$ N/m$^2$, and 0.29, respectively. The elastomeric material layer between the damper and the rail web was simulated by spring and damping elements, as shown in Figure 7. The lateral and vertical stiffness of the elastomeric material layer are 15 MN/m and 30 MN/m, respectively, and its lateral and vertical dampings are 20 kNs/m and 40 kNs/m, respectively. Parameters of rail dampers in the finite element model were obtained by field measurement [32].

As shown in Figure 8(a), the minimum effective damping ratio in the system with track type 2 increases significantly to −0.01341, compared to −0.05243, when the rail dampers are not mounted. In the leading wheelset-track system with track type 3, as shown in Figure 8(b), the minimum effective damping ratio also rises to −0.03168 from −0.09092. This means that the stability of the system is improved when the rail dampers are installed [33]. Due to the tuned frequency of rail dampers being far higher than the frequency of the unstable vibration which may lead to the formation of the 5th to 8th-order wheel OOR shapes, the

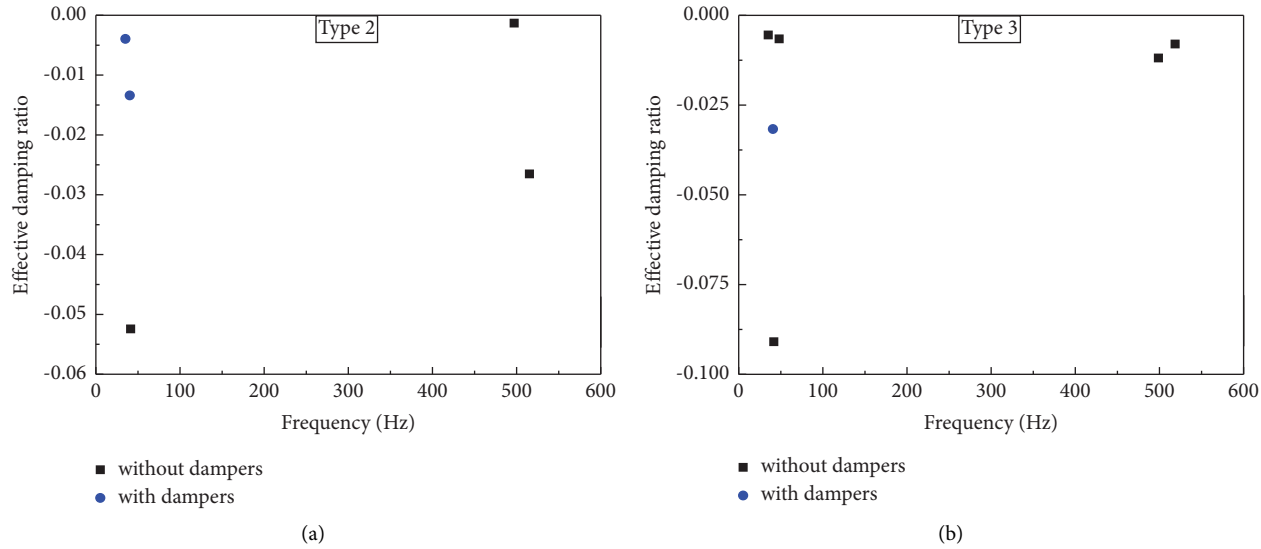


Figure 8: Effect of rail dampers on the unstable vibrations of the leading wheelset-track system with (a) track type 2 and (b) track type 3.

inhibition effect of the rail dampers on the 5th to 8th-order wheel polygonal wear is mainly because it is attached on the rail as an extra mass. Therefore, using the rail dampers can slow down the formation of the 5th to 8th-order OOR wheel induced by these unstable vibrations.

## 6. Conclusions

In the present work, three unstable vibrations that may cause the 5th to 8th-order OOR shapes on the metro leading wheel are predicted. The effect of track support structures on wheel polygonal wear is discussed, and some mitigation measures are proposed. According to simulation results, the following conclusions can be drawn:

(1) When a metro train runs on a tightly curved track, unstable vibrations may take place in the leading wheelset-track system due to the saturated wheel-rail creep forces. In the wheelset-track systems with track type 2 and type 3, the unstable vibrations of frequencies of about 35 Hz, 41 Hz, and 42 Hz may cause the periodical slide between the inner wheel tread and the low rail head, producing the 5th to 8th-order wheel OOR shapes.

(2) In the wheelset-track system with track type 2, increasing the lateral damping to 60 kNs/m or the vertical damping to 10 kNs/m can eliminate the 5th to 8th-order polygonal wear caused by the unstable vibration of frequency of about 41 Hz. In the system with track type 3, when the lateral damping rises to 60 kNs/m, wheel polygonal wear is the lowest likely to generate. When the vertical damping increases to 45 kNs/m, the 5th to 8th-order polygonal wear can be eliminated.

(3) Installing the rail dampers on the track can improve the stability of the wheelset-track system, and the rail dampers can suppress the unstable vibrations that cause the 5th to 8th-order wheel polygonal wear by adding extra mass to the rails.

This article preliminarily explores the impact of fastener damping changes in a single direction on wheel polygonal wear. In future work, the strong coupling relationship between the lateral and vertical fastener damping during the ageing process of the rail rubber pad will be studied, and its impact on wheel polygonal wear will be further analyzed.

## Data Availability

The data used to support the findings of this study are available from the corresponding author upon request.

## Conflicts of Interest

The authors declare that they have no conflicts of interest.

## Authors' Contributions

Hua Fu conceptualized and supervised the study and acquired the funding. Fei Kang investigated the data, developed the methodology, and wrote the original draft. Shanglin Liu validated the study and reviewed and edited the manuscript. Xi Kang developed the software and performed the formal analysis.

## Acknowledgments

This research was funded by the National Natural Science Foundation of China (Grant nos. 51974151 and 71771111), the Liaoning Provincial Colleges and Universities Overseas Training Project (Grant no. 2019GJWZD002), the Liaoning University Innovation Team Project (Grant no. LT2019007), and the Science and Technology Project of the Liaoning Provincial Department of Education (Grant no. LJ2019QL015).

## References

[1] B. J. Wang, S. Q. Xie, C. Y. Jiang, Q. W. Song, S. G. Sun, and X. Wang, "An investigation into the fatigue failure of metro

vehicle bogie frame," *Engineering Failure Analysis*, vol. 118, Article ID 104922, 2020.

[2] P. Wang, J. Lu, C. Y. Zhao, M. M. Chen, and M. T. Xing, "Numerical investigation of the fatigue performance of elastic rail clips considering rail corrugation and dynamic axle load," *Proceedings of the Institution of Mechanical Engineers-Part F: Journal of Rail and Rapid Transit*, vol. 235, no. 3, pp. 339–352, 2021.

[3] W. M. Zhai, X. S. Jin, Z. F. Wen, and X. Zhao, "Wear problems of high-speed wheel/rail systems: observations, causes, and countermeasures in China," *Applied Mechanics Reviews*, vol. 72, no. 6, 2020.

[4] X. S. Jin, Y. Wu, S. L. Liang, Z. F. Wen, X. W. Wu, and P. Wang, "Characteristics, mechanism, influences and countermeasures of polygonal wear of high-speed train wheels," *Journal of Mechanical Engineering*, vol. 56, no. 16, pp. 118–136, 2020.

[5] G. Q. Tao, Z. F. Wen, G. S. Chen, Y. Luo, and X. S. Jin, "Locomotive wheel polygonisation due to discrete irregularities: simulation and mechanism," *Vehicle System Dynamics*, vol. 59, no. 6, pp. 872–889, 2021.

[6] U. Spangenberg, "Variable frequency drive harmonics and interharmonics exciting axle torsional vibration resulting in railway wheel polygonisation," *Vehicle System Dynamics*, vol. 58, no. 3, pp. 404–424, 2020.

[7] X. X. Yang, G. Q. Tao, W. Li, and Z. F. Wen, "On the formation mechanism of high-order polygonal wear of metro train wheels: experiment and simulation," *Engineering Failure Analysis*, vol. 127, Article ID 105512, 2021.

[8] P. Meinke and S. Meinke, "Polygonalization of wheel treads caused by static and dynamic imbalances," *Journal of Sound and Vibration*, vol. 227, no. 5, pp. 979–986, 1999.

[9] B. Morys, "Enlargement of out-of-round wheel profiles on high speed trains," *Journal of Sound and Vibration*, vol. 227, no. 5, pp. 965–978, 1999.

[10] J. C. Nielsen, R. Lunden, A. Johansson, and T. Vernersson, "Train-track interaction and mechanisms of irregular wear on wheel and rail surfaces," *Vehicle System Dynamics*, vol. 40, no. 1–3, pp. 3–54, 2003.

[11] A. Johansson and C. Andersson, "Out-of-round railway wheels-a study of wheel polygonalization through simulation of three-dimensional wheel-rail interaction and wear," *Vehicle System Dynamics*, vol. 43, no. 8, pp. 539–559, 2005.

[12] H. Dekker, "Vibrational resonances of nonrigid vehicles: polygonization and ripple patterns," *Applied Mathematical Modelling*, vol. 33, no. 3, pp. 1349–1355, 2009.

[13] L. Wei, L. X. Zong, S. H. Luo, and X. M. He, "Research into the problem of wear creating a polygon-shaped wheel on metro trains," *Proceedings of the Institution of Mechanical Engineers-Part F: Journal of Rail and Rapid Transit*, vol. 230, no. 1, pp. 43–55, 2016.

[14] G. Q. Tao, Z. F. Wen, X. R. Liang, D. Ren, and X. Jin, "An investigation into the mechanism of the out-of-round wheels of metro train and its mitigation measures," *Vehicle System Dynamics*, vol. 57, no. 1, pp. 1–16, 2019.

[15] B. W. Wu, Q. F. Qiao, G. X. Chen et al., "Effect of the unstable vibration of the disc brake system of high-speed trains on wheel polygonalization," *Proceedings of the Institution of Mechanical Engineers-Part F: Journal of Rail and Rapid Transit*, vol. 234, no. 1, pp. 80–95, 2020.

[16] X. N. Zhao, G. X. Chen, J. Z. Lv, S. Zhang, B. W. Wu, and Q. Zhu, "Study on the mechanism for the wheel polygonal wear of high-speed trains in terms of the frictional self-excited vibration theory," *Wear*, vol. 426, pp. 1820–1827, 2019.

[17] G. X. Chen, S. Zhang, B. W. Wu et al., "Field measurement and model prediction of rail corrugation," *Proceedings of the Institution of Mechanical Engineers-Part F: Journal of Rail and Rapid Transit*, vol. 234, no. 4, pp. 381–392, 2020.

[18] W. Li, H. Y. Wang, Z. F. Wen et al., "An investigation into the mechanism of metro rail corrugation using experimental and theoretical methods," *Proceedings of the Institution of Mechanical Engineers-Part F: Journal of Rail and Rapid Transit*, vol. 230, no. 4, pp. 1025–1039, 2016.

[19] X. Kang, G. X. Chen, Q. Zhu, W. J. Ren, and B. J. Dong, "Study on wheel polygonal wear of metro trains caused by frictional self-excited oscillation," *Tribology Transactions*, vol. 64, no. 6, pp. 1108–1117, 2021.

[20] X. L. Cui, Z. Q. He, B. Huang, Y. C. Chen, Z. X. Du, and W. Qi, "Study on the effects of wheel-rail friction self-excited vibration and feedback vibration of corrugated irregularity on rail corrugation," *Wear*, vol. 477, Article ID 203854, 2021.

[21] X. Zhao, P. Zhang, and Z. F. Wen, "On the coupling of the vertical, lateral and longitudinal wheel-rail interactions at high frequencies and the resulting irregular wear," *Wear*, vol. 430, pp. 317–326, 2019.

[22] Z. Y. Xiang, W. Chen, J. L. Mo, Q. A. Liu, Z. Y. Fan, and Z. R. Zhou, "The effects of the friction block shape on the tribological and dynamical behaviours of high-speed train brakes," *International Journal of Mechanical Sciences*, vol. 194, Article ID 106184, 2021.

[23] B. W. Wu, G. X. Chen, X. Kang, and Q. Zhu, "Study on the origin of rail corrugation at a long downhill braking section based on friction-excited oscillation," *Tribology Transactions*, vol. 63, no. 3, pp. 439–452, 2020.

[24] X. L. Cui, G. X. Chen, H. G. Yang, Q. Zhang, H. J. Ouyang, and M. H. Zhu, "Study on rail corrugation of a metro tangential track with Cologne-egg type fasteners," *Vehicle System Dynamics*, vol. 54, no. 3, pp. 353–369, 2016.

[25] X. L. Cui, G. X. Chen, and H. J. Ouyang, "Study on the effect of track curve radius on friction-induced oscillation of a wheelset-track system," *Tribology Transactions*, vol. 62, no. 4, pp. 688–700, 2019.

[26] H. Ouyang, W. Nack, Y. Yuan, and F. Chen, "Numerical analysis of automotive disc brake squeal: a review," *International Journal of Vehicle Noise and Vibration*, vol. 1, no. 3/4, pp. 207–231, 2005.

[27] X. S. Jin, L. Wu, J. Y. Fang, S. Q. Zhong, and L. Ling, "An investigation into the mechanism of the polygonal wear of metro train wheels and its effect on the dynamic behaviour of a wheel/rail system," *Vehicle System Dynamics*, vol. 50, no. 12, pp. 1817–1834, 2012.

[28] J. Maes and H. Sol, "A double tuned rail damper-increased damping at the two first pinned-pinned frequencies," *Journal of Sound and Vibration*, vol. 267, no. 3, pp. 721–737, 2003.

[29] D. J. Thompson, C. J. C. Jones, T. P. Waters, and D. Farrington, "A tuned damping device for reducing noise from railway track," *Applied Acoustics*, vol. 68, no. 1, pp. 43–57, 2007.

[30] C. Y. Zhao, P. Wang, X. Sheng, and D. Meng, "Theoretical simulation and experimental investigation of a rail damper to minimize short-pitch rail corrugation," *Mathematical Problems in Engineering*, vol. 2017, Article ID 2359404, 14 pages, 2017.

[31] W. J. Qian, Y. F. Wu, G. X. Chen, and H. J. Ouyang, "Experimental and numerical studies of the effects of a rail vibration absorber on suppressing short pitch rail corrugation," *Journal of Vibroengineering*, vol. 18, no. 2, pp. 1133–1144, 2016.

[32] W. J. Qian, Z. Q. Huang, H. J. Ouyang, G. X. Chen, and H. J. Yang, "Numerical investigation of the effects of rail vibration absorbers on wear behaviour of rail surface," *Proceedings of the Institution of Mechanical Engineers-Part J: Journal of Engineering Tribology*, vol. 233, no. 3, pp. 424–438, 2019.

[33] J. Xu, X. L. Cui, H. H. Ding et al., "Optimization of vibration absorbers for the suppression of rail corrugation in the sharp curved section with Cologne-egg fasteners," *Vehicle System Dynamics*, pp. 1–16, 2023.